Dynamic equilibrium explanation for nanobubbles' unusual temperature and saturation dependence

Nikolai D. Petsev, M. Scott Shell, and L. Gary Leal

Phys. Rev. E **88**, 010402 — Published 30 July 2013

DOI: 10.1103/PhysRevE.88.010402

Dynamic Equilibrium Explanation for Nanobubbles' Unusual Temperature and Saturation Dependence

Nikolai D. Petsev, M. Scott Shell, L. Gary Leal

Department of Chemical Engineering
University of California, Santa Barbara
California 93106-5080, USA
(Dated May 9, 2013)

Abstract

The dynamic equilibrium model suggests that surface nanobubbles can be stable due to an influx of gas in the vicinity of the bubble contact line, driven by substrate hydrophobicity, that balances the outflux of gas from the bubble apex. Here, we develop a new formulation of this mechanism that predicts rich behavior in agreement with recent experimental measurements. Namely, we find that stable nanobubbles exist in narrow temperature and dissolved gas concentration ranges, that there is a maximum and minimum possible bubble size, and that nanobubble radii decrease with temperature.

Body

Interfacial nanobubbles form on solid hydrophobic substrates when immersed in water with dissolved gas (e.g. nitrogen, oxygen, argon, etc.), and are spherical-cap-shaped gaseous domains with heights of ~20 nm and widths of ~100 nm [1–18]. Due to the small radius of curvature, a typical nanobubble has extremely high internal capillary pressure (~2-10 atm), which provides a substantial driving force for dissolution. Simple diffusion arguments therefore suggest microsecond dissolution times, yet nanobubbles have been observed to persist for days [16]. This mysterious stability represents a fundamental problem in nano-scale interfacial phenomena, even though nanobubbles have become important for increasing slip along surfaces [19–22], removing biological fouling [23], and in a host of other technologies [24,25].

Why are nanobubbles stable? A *dynamic* equilibrium mechanism proposed by Brenner and Lohse [26] has received increasing attention, and it offers an alternative to earlier ideas like contamination that now appear insufficient as a complete explanation [27–29]. This model (Fig. 1a) suggests that the outflux of gas from the top of the bubble is recirculated and re-absorbed near the three-phase contact line due to the attraction and enrichment of dissolved gas at the hydrophobic substrate. It was later suggested that the recirculation currents are induced by shear stresses imposed on the liquid-gas interface due to Knudsen diffusion of the gas inside the bubble [30]. While the ultimate driving force for recirculation is unknown at present, one possibility is subtle temperature gradients due to evaporation [25]. It is worthwhile to note that another transport-based explanation recently proposed that nanobubble lifetimes are due to slow gas diffusion (a 'traffic jam' effect) across the liquid film [31]; however, it is yet unclear whether this provides the full picture, since convective currents would dramatically expedite mass transfer in real experiments. Other recent work suggests nanobubbles may exist in a thermodynamically metastable state due to contact line pinning [32], although bubbles have been observed to adjust their lateral size [33] and may be moved along the substrate using the tip of an atomic force microscopy apparatus [7,34].

In this Rapid Communication, we develop a new formulation of the dynamic equilibrium mechanism and show that a stability analysis explains many unexpected experimental observations regarding the influence of temperature and gas saturation on nanobubbles. In particular, there is remarkable qualitative agreement with the results of Seddon et al. [35], who reported that nanobubbles nucleate in a narrow temperature range, and that the total volume of nanobubbles decreases with temperature. Moreover, by using a realistic, empirical potential for

the hydrophobic attraction, we find that the dynamic equilibrium mechanism does not require unphysical parameters for a contact angle correction, as in the original model.

Our model treats the influx and outflux components of the dynamic mechanism independently by assuming that the relevant length scale for the outflux (which is $O(R)$, where R is bubble radius) is much larger than that for the influx (which is on the order of the thickness of the gas-enrichment layer, around a nanometer). Moreover, this approach focuses on the region immediately surrounding the bubble, where mass transfer is diffusion-limited, rather than the full convective recirculation problem. Given the observed small contact angles of nanobubbles [7,12,18,34,36], we first approximate the steady-state diffusive gas outflux using a completely flat bubble, which is readily solved using oblate spheroids [37,38],

$$J_{out}(R) = 4DR\left[C(R) - C_\infty\right] \tag{1}$$

Here, D is the diffusion constant for the gas in the liquid, R is the bubble radius, $C(R)$ is the liquid-side gas concentration at the bubble surface, and C_∞ is its concentration infinitely far away. C_∞ can be related to the ambient pressure P_0 if the bulk liquid is open to the atmosphere and saturated, with $C_\infty = k_H P_0$, where k_H is a temperature-dependent Henry's law constant. Similarly, $C(R) = k_H\left(2\gamma \sin\theta_c / R + P_0\right)$ through the Young-Laplace equation, where θ_c is the bubble contact angle. γ gives the surface tension, here described by the Eötvös relation with parameters for an air-water interface. Because experiments [7,12,18,34,36] suggest the contact angle of small bubbles deviates from the macroscopic value (e.g., due to surface inhomogeneities or line-tension effects [36,39–44]), we introduce an R-dependent θ_c [26,36]:

$$\cos\theta_c = \cos\theta_\infty - \frac{\cos\theta_\infty - \cos\theta_0}{1 + R/\delta} \tag{2}$$

In this expression, θ_∞ is the macroscopic gas-side contact angle, which we take to be 40°. θ_0 is the contact angle as $R \to 0$, and equals zero. δ sets the length scale for the onset of microscopic corrections; we pick $\delta = 3.2$ nm to yield realistic predictions, in agreement with experimental fits to this parameter [36]. Because we use a more realistic hydrophobic interaction (described shortly), we avoid the unrealistically high values of δ previously required for the dynamic equilibrium model [26].

The influx is determined by $J_{in} = -D\int \nabla C \cdot \mathbf{n} dS$, where the integral is over the bubble surface. Gas molecules experience an attractive interaction with the hydrophobic substrate according to a potential $\Phi(z)$; therefore, using $D\nabla C = -C\nabla\Phi/\zeta$ for diffusion in a field, we obtain

$$J_{in}(R) = \frac{C(R)}{\zeta}\int \nabla\Phi \cdot \mathbf{n} dS \approx \frac{C(R)}{\zeta}\iint \left[\frac{d\Phi}{dz}\right]_{z=h(r)} \cos\theta_c r dr d\theta \tag{3}$$

where $\zeta = k_B T / D$ is the solute mobility and h is the shape function for the bubble in the vicinity of the contact line, which we approximate as $h(r) = (R - r)\tan\theta_c$. Unlike previous work [26], we choose a continuous, decaying exponential potential proposed from experiments to describe

the hydrophobic attraction [45], $\Phi(z) = -Ae^{-Bz}$. Eq. 3 can be evaluated analytically by assuming that $\Phi(z)$ decays rapidly to yield

$$J_{in}(R) \approx \frac{2\pi DC(R) A \cos\theta_c}{k_B T} \left[\frac{1 - BR\tan\theta_c}{B\tan^2\theta_c} \right] \tag{4}$$

It is worthwhile to note that for very small values of R and θ_c, J_{in} becomes positive and inaccurate since the separation of length scales and the linear shape approximation fail when the bubble radius or height approach the potential decay length, which is known from experiment to be B^{-1} = 1 nm [45]. The magnitude of the attractive potential at the solid-liquid interface (set by A) is treated as approximately constant, and a value of $A \approx 0.40$ kcal/mol was found to yield realistic results. This value is on the order of magnitude of the hydrophobic interaction between two methane molecules in water [46], and similar to the values used by Brenner and Lohse [26].

Fig. 1b shows that the net flux of gas into the bubble, normalized by *C(R)*, can have a non-monotonic dependence on bubble radius that is quite sensitive to temperature. These results are shown for the fully saturated case. Stable bubbles of radius R^* occur when $j_{out}(R^*) + j_{in}(R^*) = j_{net}(R^*) = 0$ and $dj_{net}(R^*)/dR > 0$. The derivative condition must be satisfied so that a bubble will return to its original size in response to small perturbations to radius (i.e., perturbations to smaller R cause a net influx, $j_{net} < 0$, and vice versa). Fig. 1b illustrates that there is only one unstable point at T = 26 °C, but at T = 36 °C, a stable point occurs at R^* = 40 nm in addition to two unstable ones. As temperature is raised, the stable point shifts towards smaller bubble radii, and ultimately vanishes at T = 56 °C. Therefore, this

formulation of the dynamic equilibrium model suggests that, for fully saturated liquid in contact with a hydrophobic substrate, stable nanobubbles exist in a narrow range of temperatures, with a minimum and maximum possible bubble size associated with the maximum and minimum temperatures, respectively. The exact breadth of the temperature range depends on the specific parameters used.

Surprisingly, the temperature dependence of gas solubility does not affect nanobubbles in this model, since both influx and outflux scale linearly with k_{H} . Surface tension only weakly influences nanobubbles since it does not vary dramatically over the considered temperature ranges. The temperature dependence of R^* (Fig. 2a) is primarily introduced through the influx, which scales as $\sim 1/T$ due to the solute mobility. With rising temperature, solute mobility increases and dissolved gas molecules more readily overcome the attractive influence of the hydrophobic potential, which shrinks the gas-rich region (as evidenced by the solute concentration profile in the absence of a bubble, given by $C(z) = C_\infty \exp\left[-\Phi(z)/k_B T\right]$). This lowers the influx and the outflux shrinks bubbles until the fluxes balance again. Above some temperature ($T_{\max} \approx 48$ °C), the effect of the potential falls to levels where the influx is too small to ever balance the outflux. Bubbles above this temperature will thus shrink and dissolve. Similarly, below some temperature ($T_{\min} \approx 35$ °C), the action of the attractive field dominates and bubbles grow without bound until the gas is locally depleted or the thermodynamic work required to sustain the influx becomes too great. If a bubble becomes sufficiently large, it may also detach from the substrate due to buoyancy.

The result in Fig. 2a qualitatively agrees with the observations of Seddon et al [35] for the case of a saturated liquid in thermal equilibrium with the substrate. The model presented in this Rapid Communication accounts for the sudden appearance of a high density of nanobubbles

at a minimum critical temperature, the finite temperature range where bubbles were observed, and why bubbles at lower temperatures appear coarser. The decrease in bubble size (Fig. 2a), coupled to an experimentally observed increase in bubble number density with temperature [8,12], might also explain the observed maximum in the total nanobubble volume versus temperature [33,36]. Furthermore, the prediction of larger bubbles at lower temperatures possibly accounts for the increase in average nanobubble separation with decreasing temperature [33], since larger bubbles require a greater surrounding unperturbed gas-rich region.

We do note that other studies have reported more complicated behavior. Recent work finds non-monotonic changes in the average nanobubble radius with decreasing temperature [33,47]. Differences between the model predictions and these observations are possibly due to the complicated temperature dependence of the hydrophobic attractive potential, which we ignore here. The complex nature of this potential may explain the sensitivity of bubble morphology to the hydrophobicity parameter A (Fig 2a) in our simple model. This sensitivity may also be partly responsible for the earlier difficulty in reproducibility among nanobubble experiments [35].

Beyond temperature, a second important control parameter is the dissolved gas concentration (C_∞), and Fig. 2b shows how it affects the stable radius R^*. There exist large regions in the space of temperature and saturation where stable bubbles cannot exist, which may provide further interpretation for reproducibility problems. Where they do exist, lowering C_∞ reduces bubble size since this elevates the driving force for outflux but has no effect on the influx (the concentration immediately next to the bubble at the surface is unaffected), as also described by Ref. [26]. As previously, perturbing bubbles to a state outside of the viable region will lead to bubbles either dissolving or growing until the influx expires. The result in Fig. 2b is

in agreement with experiments indicating that bubbles in supersaturated fluid are larger than those in undersaturated conditions [12]. Interestingly, this model also suggests that there may be middle-range temperatures (e.g., 45 °C in Fig. 2b) at which the stable bubble radius is quite insensitive to saturation, as reported by Ref. [34], while near the lower temperature limit it can be rather pronounced.

In the model described thus far, we constrained the contact angle such that it depends explicitly on the bubble radius. We now relax the ad hoc constraint imposed by Eq. 2 and examine the stability of bubbles to perturbation in θ_c. Fig. 3 shows the net flux versus both contact angle and radius, where the two are treated as independent. The solid black curve corresponds to the points where the fluxes balance ($j_{net} = 0$). For a fixed contact angle, it is not possible to generate stable bubbles with respect to perturbation in *R*; a bubble perturbed to the left of the stable curve at constant angle enters a region where the sum of fluxes is positive and the outflux dominates, and thus will shrink and disappear.

Bubbles are stable, however, to perturbations in θ_c at fixed *R*. If a bubble pinned at the contact line begins to dissolve and lose vertical height, the contact angle decreases, which leads to an increase in the bubble surface area that is situated within the gas-rich region (which has fixed width). Ultimately, this increases the influx and stabilizes the bubble. The size of a pinned bubble exhibits the same qualitative behavior as described previously, with increases in *T* leading to smaller θ_c^*, and increases in saturation leading to a taller bubble with larger θ_c^*, as observed by Ref. [48]. Without the constraint posed by Eq. 2, however, the model no longer predicts physical limits on the temperature and saturation ranges where bubbles can exist.

Note that the stable contact angle θ_c^* is less than 30° for a wide range of bubble radii in Fig. 3, as reported in numerous experimental nanobubble studies. Furthermore, a bubble

perturbed in *any* arbitrary direction from the black curve in Fig. 3 may be stable if the bubble's response to perturbation in θ_c is more rapid than its response to perturbation in *R*. This is likely to be the case since surface roughness and inhomogeneities will inevitably lead to at least partial contact line pinning. With this in mind, the predicted curve indicating possible combinations of θ_c and *R* that yield stable bubbles (solid black curve) looks remarkably similar to the ad hoc *R*-dependent contact angle constraint that we applied previously, which is shown for comparison as the dashed curve. Therefore, this model suggests that a possible *dynamic* phenomenon may also explain deviations from macroscopic contact angles in nanobubbles.

Even if the dynamic equilibrium model cannot ultimately describe long-term stability, it may still be relevant to the nucleation process since it poses a means by which bubbles may grow. As indicated by the stability analysis, a bubble will tend towards a preferred radius determined by the solution conditions, and may begin as a fluctuation in gas density that inflates via the dynamic equilibrium mechanism until it reaches this size. At this point, the influx may expire and the bubble might be stabilized by different means, such as the diffusive traffic jam effect described by Weijs and Lohse [31], contact line pinning [32], or some other hitherto undiscovered means. This would also explain why our predictions agree with experimental data where bubbles were explicitly nucleated for every data point.

While the dynamic equilibrium model predicts rich behavior, it may also have limitations. First, the source of energy for recirculation remains an unresolved issue. Also, the model cannot explain the presence of nanoscopic bubbles along hydrophilic substrates. A transient localized gas-rich layer, similar to those in systems with hydrophobic substrates, can develop along a hydrophilic interface during solvent exchange [10], but it is unclear what mechanism might draw gas solute molecules from this gas-rich region into the bubble.

Furthermore, a recent study [49] using tracer particles in the vicinity of nanobubbles reported no evidence for an influx near the contact line. However, the particles used are comparable in diameter to the actual nanobubbles, and it is not clear whether velocities localized to a region just a few nanometers over the substrate can be resolved with this technique. Lastly, a study using optical interference-enhanced reflection microscopy [50] reports that nanobubble sizes remained constant over a broad temperature range, in conflict with other experimental studies and our predictions. Ultimately, a more consistent experimental picture is needed under varying conditions, but expounding the detailed behaviors and implications of models like the dynamic equilibrium one remains an essential step in guiding such efforts and in building a deeper understanding of the phenomena at play, even if eventually they are not the full picture.

In summary, we demonstrated through a stability analysis that the dynamic equilibrium hypothesis for nanobubble stability indicates that nanobubbles should only be observed in a narrow range of temperatures and that their radii should decrease monotonically with temperature. Both predictions have been observed in experiment. Interestingly, the model also predicts large regions of temperature-gas saturation state space where nanobubbles cannot be observed. We believe a thorough understanding of the consequences of this hypothesis may finally settle whether it is a valid picture of nanobubble stability or nucleation through future experimental work.

The authors gratefully acknowledge the support of the National Science Foundation (Award Number CBET-1256838).

References

[1] P. Ball, Nature **423**, 25 (n.d.).
[2] O. I. Vinogradova, N. F. Bunkin, N. V. Churaev, O. A. Kiseleva, A. V. Lobeyev, and B. W. Ninham, Journal of Colloid and Interface Science **173**, 443 (1995).
[3] J. W. G. Tyrrell and P. Attard, Phys. Rev. Lett. **87**, 176104 (2001).
[4] P. Attard, Advances in Colloid and Interface Science **104**, 75 (2003).
[5] J. L. Parker, P. M. Claesson, and P. Attard, J. Phys. Chem. **98**, 8468 (1994).
[6] M. Holmberg, A. Kühle, K. A. Mørch, and A. Boisen, Langmuir **19**, 10510 (2003).
[7] A. C. Simonsen, P. L. Hansen, and B. Klösgen, Journal of Colloid and Interface Science **273**, 291 (2004).
[8] X. H. Zhang, X. D. Zhang, S. T. Lou, Z. Zhang, J. L. Sun, and J. Hu, CAS OpenIR **20**, (2004).
[9] A. Agrawal, J. Park, D. Y. Ryu, P. T. Hammond, T. P. Russell, and G. H. McKinley, Nano Lett. **5**, 1751 (2005).
[10] X. H. Zhang, N. Maeda, and V. S. J. Craig, Langmuir **22**, 5025 (2006).
[11] L. Zhang, Y. Zhang, X. Zhang, Z. Li, G. Shen, M. Ye, C. Fan, H. Fang, and J. Hu, Langmuir **22**, 8109 (2006).
[12] S. Yang, S. M. Dammer, N. Bremond, H. J. W. Zandvliet, E. S. Kooij, and D. Lohse, Langmuir **23**, 7072 (2007).
[13] B. M. Borkent, S. M. Dammer, H. Schönherr, G. J. Vancso, and D. Lohse, Phys. Rev. Lett. **98**, 204502 (2007).
[14] X. H. Zhang, A. Khan, and W. A. Ducker, Phys. Rev. Lett. **98**, 136101 (2007).
[15] S. Yang, E. S. Kooij, B. Poelsema, D. Lohse, and H. J. W. Zandvliet, EPL (Europhysics Letters) **81**, 64006 (2008).
[16] X. H. Zhang, A. Quinn, and W. A. Ducker, Langmuir **24**, 4756 (2008).
[17] S.-T. Lou, Z.-Q. Ouyang, Y. Zhang, X. Li, J. Hu, M. Li, and F.-J. Yang, Journal of Vacuum Science Technology B: Microelectronics and Nanometer Structures **18**, 2573 (2000).
[18] N. Ishida, T. Inoue, M. Miyahara, and K. Higashitani, Langmuir **16**, 6377 (2000).
[19] Y. Wang and B. Bhushan, Soft Matter **6**, 29 (2009).
[20] Y. Wang, B. Bhushan, and X. Zhao, Langmuir **25**, 9328 (2009).
[21] D. C. Tretheway and C. D. Meinhart, Physics of Fluids **16**, 1509 (2004).
[22] E. Lauga and M. P. Brenner, Phys. Rev. E **70**, 026311 (2004).
[23] Z. Wu, H. Chen, Y. Dong, H. Mao, J. Sun, S. Chen, V. S. J. Craig, and J. Hu, Journal of Colloid and Interface Science **328**, 10 (2008).
[24] W. B. Zimmerman, V. Tesař, and H. C. H. Bandulasena, Current Opinion in Colloid & Interface Science **16**, 350 (2011).
[25] J. R. T. Seddon, D. Lohse, W. A. Ducker, and V. S. J. Craig, ChemPhysChem **13**, 2179 (2012).
[26] M. P. Brenner and D. Lohse, Phys. Rev. Lett. **101**, 214505 (2008).
[27] W. A. Ducker, Langmuir **25**, 8907 (2009).
[28] S. Das, J. H. Snoeijer, and D. Lohse, Phys. Rev. E **82**, 056310 (2010).
[29] X. Zhang, M. H. Uddin, H. Yang, G. Toikka, W. Ducker, and N. Maeda, Langmuir **28**, 10471 (2012).
[30] J. R. T. Seddon, H. J. W. Zandvliet, and D. Lohse, Phys. Rev. Lett. **107**, 116101 (2011).

[31] J. H. Weijs and D. Lohse, Phys. Rev. Lett. **110**, 054501 (2013).
[32] Y. Liu and X. Zhang, The Journal of Chemical Physics **138**, 014706 (2013).
[33] R. P. Berkelaar, J. R. T. Seddon, H. J. W. Zandvliet, and D. Lohse, ChemPhysChem **13**, 2213 (2012).
[34] X. H. Zhang, G. Li, N. Maeda, and J. Hu, Langmuir **22**, 9238 (2006).
[35] J. R. T. Seddon, E. S. Kooij, B. Poelsema, H. J. W. Zandvliet, and D. Lohse, Phys. Rev. Lett. **106**, 056101 (2011).
[36] M. A. J. van Limbeek and J. R. T. Seddon, Langmuir **27**, 8694 (2011).
[37] P. A. Bobbert, M. M. Wind, and J. Vlieger, Physica A: Statistical Mechanics and Its Applications **141**, 58 (1987).
[38] See Supplemental Material at [] for a detailed derivation of Eq. 1, as well as a sensitivity analysis of the described model.
[39] A. Checco, P. Guenoun, and J. Daillant, Phys. Rev. Lett. **91**, 186101 (2003).
[40] A. Checco, H. Schollmeyer, J. Daillant, P. Guenoun, and R. Boukherroub, Langmuir **22**, 116 (2006).
[41] P. Jakubczyk and M. Napiórkowski, Journal of Physics: Condensed Matter **16**, 6917 (2004).
[42] D. Li, Colloids and Surfaces A: Physicochemical and Engineering Aspects **116**, 1 (1996).
[43] N. Kameda and S. Nakabayashi, Chemical Physics Letters **461**, 122 (2008).
[44] N. Kameda, N. Sogoshi, and S. Nakabayashi, Surface Science **602**, 1579 (2008).
[45] J. N. Israelachvili, *Intermolecular and Surface Forces, Third Edition*, 3rd ed. (Academic Press, 2010).
[46] S. Shimizu and H. S. Chan, The Journal of Chemical Physics **113**, 4683 (2000).
[47] Z. Xue-Hua, L. Gang, W. Zhi-Hua, Z. Xiao-Dong, and H. Jun, Chinese Physics **14**, 1774 (2005).
[48] X. Zhang, D. Y. C. Chan, D. Wang, and N. Maeda, Langmuir **29**, 1017 (2013).
[49] C. U. Chan and C.-D. Ohl, Phys. Rev. Lett. **109**, 174501 (2012).
[50] S. Karpitschka, E. Dietrich, J. R. T. Seddon, H. J. W. Zandvliet, D. Lohse, and H. Riegler, Phys. Rev. Lett. **109**, 066102 (2012).

Figures

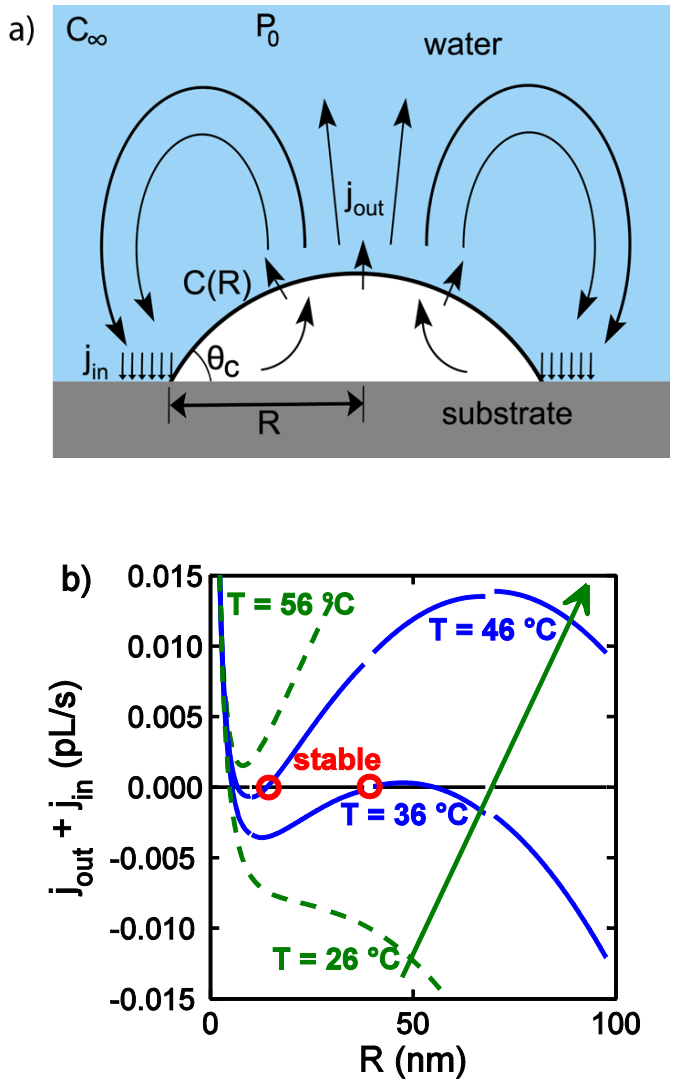

FIG. 1 (color online). (a) Schematic of the dynamic equilibrium mechanism for nanobubble stability. (b) Sum of influx and outflux, scaled by the concentration at the bubble surface ($j_{out} = J_{out} / C(R)$, $j_{in} = J_{in} / C(R)$), versus bubble radius for several different temperatures. The blue (solid) curves denote temperatures at which stable points are found.

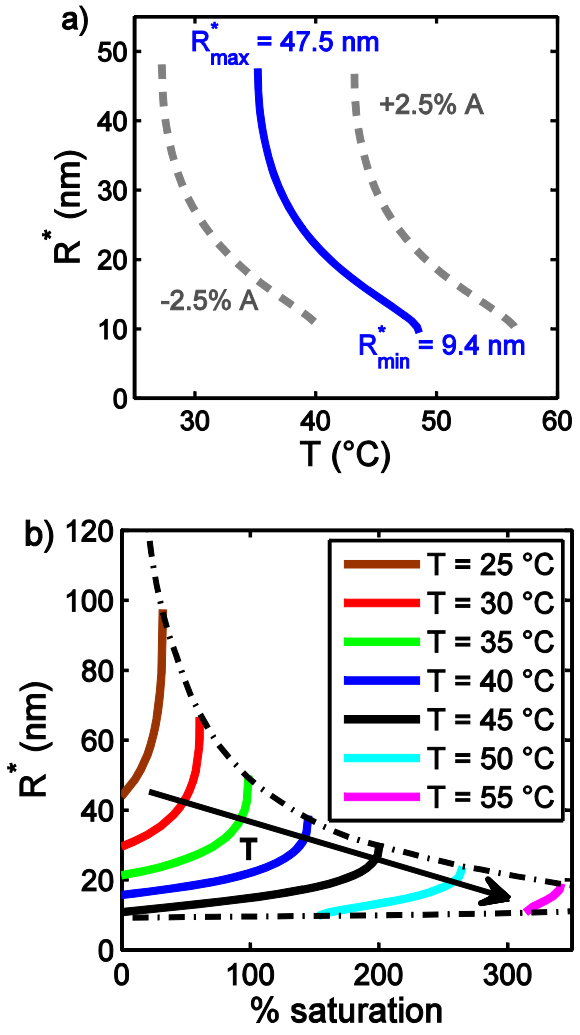

FIG. 2 (color online). (a) Stable bubble radius versus temperature according to dynamic equilibrium model, shown for different values of *A* (dashed curves). (b) Stable bubble radius versus solute concentration for several different temperatures. Arrow indicates direction of increasing *T*.

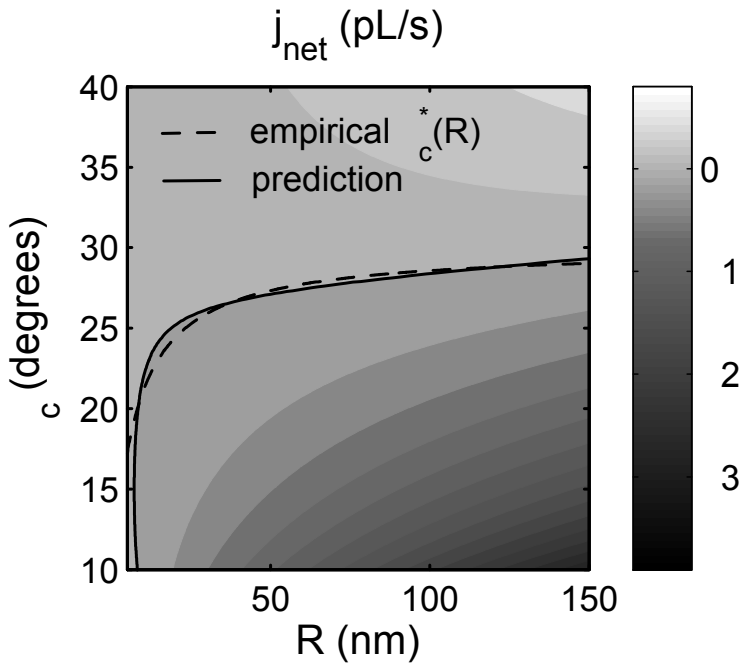

FIG. 3 (color online). Sum of influx and outflux versus both radius and contact angle for $T = 27$ °C. Points where the fluxes balance are shown by the solid curve. The dashed curve is Eq. 2, with $\theta_\infty = 30°$ and $\delta = 10$ nm.